Numerical Simulation of Projectiles in Detonable Gases

SuYeon Moon , ChooungWon Lee, and ChangHyun Sohn

Abstract

A numerical parametric study is conducted to simulate shock-induced combustion with a variation in freestream conditions. The analysis is limited to inviscid flow and includes chmical nonequilibrium. A steady combustion front is established if the freestream Mach number is above the Chapman-Jouguet speed of the mixture. On the other, an unsteady reaction front is established if the freestream Mach number is below or at the Chapman-Jouguet speed of the mixture. The three cases have been simulated for Machs 4.18, 5.11, and 6.46 with a projectile diameter of 15 mm. Machs 4.18 and 5.11 shows an unsteady reaction front, whereas Mach 6.46 represents a steady reaction front. Thus Chapman-Jouguet speed is one of deciding factor for the instabilities to trigger. The instabilities of the chemical front with a variation of projectiles diameters will be investigated

Key Words: Finite Element Method, Bow Shock, Reaction Front, Induction Zone, Mixed Explicit Implicit method

1. Introduction

Some of the applications of supersonic research are the proposed hypersonic plane, the ram accelerator and Trans Atmospheric Vehicles. All of these vehicles rely on air-breathing propulsion. The airbreathing engine removes the requirement to carry an oxidizer inside the vehicle. Further, there is a substantial saving in weight and, therefore, the payload is higher. An efficient propulsion system at hypersonic speeds requires that combustion take place at supersonic speed, i.e., combustion at supersonic mean airstream speed. The supersonic combustion speed is required for airbreathers at high Mach numbers to reduce the unacceptable losses associated with inlet deceleration to subsonic conditions. The scramjet [1, 2] is an integrated airframe-propulsion concept for a hypersonic airplane. Significantly increased propulsion efficiency in the Mach 6 to 15 range may be provided by the conventional diffusion-burning, air-breathing scramjet. For airbreathers above Mach 15, another propulsion approach is required, e.g., greatly enhanced (reduced loss) conventional scramjet and detonation wave engines.

Ballistic range experiments performed in the 1960's and 1970's provide an excellent source for studying supersonic combustion/detonation. The physics of these ballistic range flows are predominantly driven by reaction kinetics and convection phenomena. Any discrepancy between the experimental data and numerical calculations can be attributed to either numerical errors or the improperly modeled chemical kinetics.

Zeldovich [3] suggested that combustion can be stabilized by the shock wave produced by bodies moving at supersonic speeds in combustible mixtures at various level of overdrive. In these experiments, projectiles were fired in different premixed fuel-air mixtures, and detonation structures around the projectiles were recorded. Lehr's [4] experimental ballistic range shadowgraphs for Mach 5.11 and Mach 6.46 are shown in Figs. 1 and 2, respectively. A free-stream temperature of 292 K and a pressure of 42663.2N/m^2 are used along with a stoichiometric mixture of hydrogen and air in both cases. In Fig. 1 the projectile velocity is Mach 5.11 which is also the Chapman-Jouget velocity of the mixture.

Several researchers [5-9] have recently attempted to numerically simulate Lehr's ballistic range experiments. Youngster et al. [5] and Lee and Deiwart [6] simulated Lehr's experimental data for Machs 4.18, 5.11 and 6.46. They used Euler equations coupled with species equations to capture the shock and the reaction front. The reaction model used was a hydrogen-air mixture of six species and an inert gas such as Argon or Nitrogen and eight reactions. However, the flow field was not well resolved. 32×32 and 57×41 size grids were used in their blunt body calculations used. respectively. These grids were not sufficient to resolve the flow field correctly. Wilson and MacCormack [7] conducted a detailed numerical investigation of the shock-induced combustion phenomena. Euler equations and a 13-species. 33-reactions chemistry model was used. The validity of the reaction models and the

* Kyungpook National University

importance of grid resolution needed to properly model the flow physics were also shown. Highly resolved calculations for Lehr's Mach 5.11 and Mach 6.46 cases with an adaptive grid were performed. The calculations were not time accurate: therefore, the unsteady behavior was not captured. Sussman and Wilson [8] also studied the instabilities in the reaction front for a Mach number of 4.79. Euler equations and a 13-species, 33-reactions chemistry model was again used. They have proposed a new formulation based on logarithmic transformation. The number of grid points needed to properly resolve the reaction front is greatly reduced. They successfully simulated the unsteady case. However, the frequency was slightly underpredicted. Matsuo and Fujiwara [9] have studied the instabilities of shock-induced combustion around an axisymmetric blunt body will Euler equations and a simplified two-step chemistry model. The growth of periodic instabilities by a series of simulations with various tip radii was investigated; these periodic instabilities are related to shock-standoff distance and induction length. They proposed a new model based on McVey and Toong's model [10] that explained the instabilities in the reaction front. The appearance or disappearance of the instabilities in the structure of the reaction front with various Mach number has been studied in detail, and a satisfactory explanation of the various flow phenomena have been explained by the wave-interaction model by McVey and Toong. The instabilities originate in the induction zone that separates the bow shock and the exothermic reaction front in the nose region of the flow field and then spreads outwards.

2. MEI Formulation

For the general purpose program considering the compressible turbulent flows, we write the conservation form of the Navier-Stokes system of equations as

$$\frac{\partial \mathbf{U}}{\partial t} + \frac{\partial \mathbf{F}_i}{\partial x_i} = \mathbf{0} \tag{1}$$

where $\mathbf{U}$ and $\mathbf{F}_i$ denote the conservation flow variables, convection flux variables, respectively,

$$\mathbf{U} = \begin{bmatrix} \rho \\ \rho v_j \\ \rho E_k \end{bmatrix} \qquad \mathbf{F}_i = \begin{bmatrix} \rho v_i \\ \rho v_i v_j + p\delta_{ij} \\ \rho E v_i + p v_i \end{bmatrix}$$

Mixed explicit-implicit finite element methods are formulated in [11].

3. Chemical Kinetics and Thermodynamics Model

The right hand side of the species equations contain source terms (w_i). These terms represent the generation or destruction of species i due to chemical reactions. The stoichiometric equation of a set of N_R elementary reactions involving N_s species is

$$\sum_{i=1}^{N_s} \nu'_{i,j} M_i \quad \Longleftarrow \quad \sum_{i=1}^{N_s} \nu''_{i,j} M_i \tag{2}$$

where $\nu'_{i,j}$ and $\nu''_{i,j}$ are the stoichiometric coefficients of species i for the reaction step j appearing as a reactant and as a product, respectively, and M_i is the chemical symbol for species i. The forward reaction rate constants $K_{f,j}$ and the backward reaction rate $K_{b,j}$ are functions of the temperature and are given by the Arrhenius form,

$$K_{f,j} = A_{fj} T^{B_{fj}} \exp(-E_{fj}/RT)$$
$$K_{b,j} = A_{bj} T^{B_{bj}} \exp(-E_{bj}/RT) \tag{3}$$

The rate of production of species i for the reaction step j is given by

$$w_i = (\nu''_{i,j} - \nu'_{i,j})\hat{w}_j \tag{4}$$

with the net forward rate of the j th reaction defined as

$$\hat{w}_k = K_{f,j} \prod_{i=1}^{N_s} C_i^{\nu'_{i,j}} - K_{b,j} \prod_{i=1}^{N_s} C_i^{\nu''_{i,j}} \tag{5}$$

Thus, the reaction rate assume the form

$$w_k = M_k \sum_{j=1}^{N_R} (\nu''_{i,j} - \nu'_{i,j})(K_{f,j} \prod_{i=1}^{N_s} C_i^{\nu'_{i,j}} - K_{b,j} \prod_{i=1}^{N_s} C_i^{\nu''_{i,j}}) \tag{6}$$

where C_i is the molar concentration of species i.

In the present study, the finite rate reactions of hydrogen-air (18 steps and 2steps) in applications to various combustors are considered. A detailed reaction models for the 18steps hydrogen-air are shown in Table 1. The specific heat at constant

pressure, C_p , is determined by fourth-order polynomials of temperature,

$$C_{pk} = A_k + B_k T + C_k T^2 + D_k T^3 + E_k T^4 \qquad (7)$$

The coefficients of these polynomials are accessed from a generalized data bank of JANNAF Table. The specific heat of the gas mixture is obtained by concentration weighting of each species. The temperature is related to the static enthalpy from the relation

4. Results and Discussions

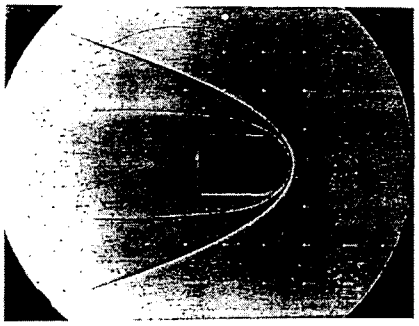

Figure 1 Shadowgraph of a spherical node projectile moving at Mach 5.11 into a premixed stoichiometric hydrogen-air mixture

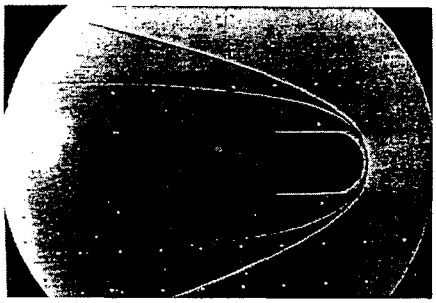

Figure 2 Shadowgraph of a spherical node projectile moving at Mach 6.46 into a premixed stoichiometric hydrogen-air mixture

When a blunt body is moving through a reactive mixture at a hepersonic speeds, a bow shock is formed ahead of the body, and the temperature of the fuel –air mixture after the bow shock is sufficiently high to initiate the reaction. Once ignition starts, chemical energy is released and another discontinuity know as the reaction front is formed. The flow attains equilibrium due to large residence time in the stagnation zone, the flow is in a state of nonequilibrium. The premixed fuel oxidizer mixture is taken as $2H_2+O_2+3.76N_2$ and the stoichiometric chemical reaction for the system can be written as

$$2H_2+O_2+3.76N_2 \rightarrow 2H_2O+3.76N_2$$

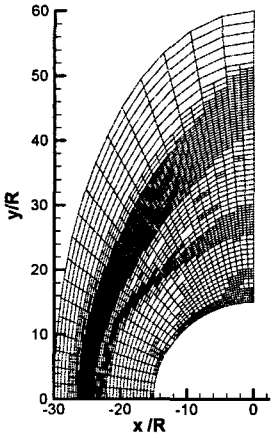

(a) Adaptive Meshes

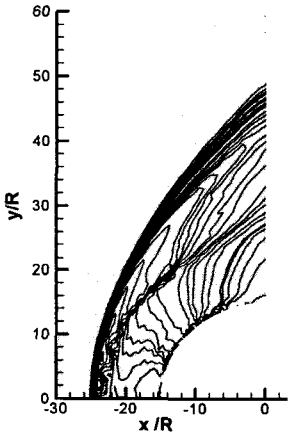

(b) Density

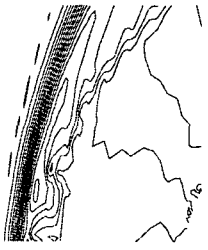

(c) Enlarged view of Temperature Contours

Figure 3 Adaptive Meshes and Contours of Temperature and Density for March 4.18 and Projectile Diameter 15 mm

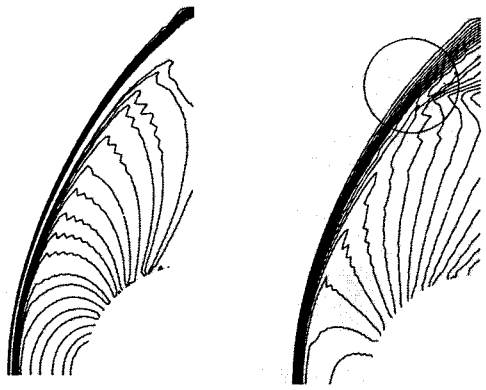

(a) Temperature (b) Density

Figure 4 Contours of Temperature and Density for March 5.11 and Projectile Diameter 15 mm

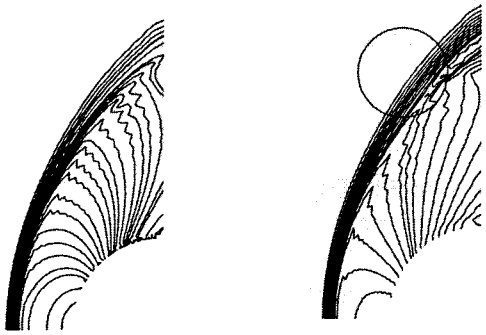

(a) Temperature (b) Density

Figure 5 Contours of Temperature and Density for March 6.46 and Projectile Diameter 15 mm

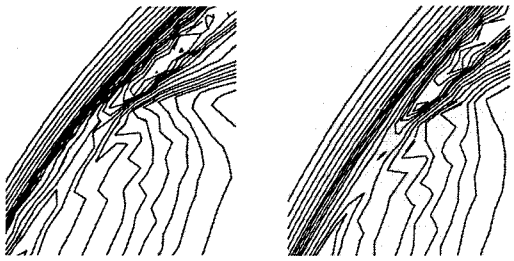

(a) Density for Mach 5.11 (b) Density for Mach 6.46 around the reaction front

Figure 6 Comparisons of Enlarged Contours of Densities for Mach 5.11 and 6.46

For the present stoichiometric hydrogen-air mixture, the Chapman-Jouget(C-J) velocity is Mach 5.11. Thus for the Mach 6.46 case, the projectile speed is significantly above the detonation velocity of the mixture. If the freestream velocity of the projectile is around the C-J detonation of the mixture, unsteady flow phenomenon can occur. Thus, the freestream velocity becomes the parameters: Mach=4.18, 5.11, and 6.46. The projectile diameter is 15 mm. Figure 3 demonstrates adaptive meshes, contours of temperature and density and enlarged view of temperature contours for Mach 4.18 and projectile diameter 15 mm. Calculations are performed for a grid with 40 points in the circumferential direction and 40 points in the normal direction. The refinements of the meshes are applied to the flowfield as the steady state reaches, which is presented by Figure 3(a). The features of Figure 3(b) are that a small induction distance occur due to the post-shock temperature near the stagnation zone. The induction distance is abruptly increased due to weak shock strength and post-shock temperature as flows proceed away from the stagnation zone. It is observed that oscillations are found in the reaction front in Figure 3(c) which is a magnification of the circle in Figure 3(b). Figure 4 shows the contour plots of density and temperature for the Mach 5.11. The bow shock is very smooth, but the reaction front shows oscillations, which is more clearly seen in the enlarged view as shown in Figure 6. The bow shock and the reaction front are separated from each other by the induction distance. The separation is minimum at the stagnation line and increases away form it due to low post-shock temperature away from the stagnation region. The incoming Mach number is increased to 6.46, making it superdetonative case, maintaining the projectile diameter of 15 mm as in case above.

The bow shock and the reaction front can be also seen in the contours of the temperature and density in Figures 5(a) and (b). They are coupled with each other near the stagnation line and up to about 60 degrees from the nose, at which point they begin to decoupled from each other by the induction distance. This can be explained by the fact that shock is almost normal near the stagnation line and the post-shock temperature is maximum. For Mach 6.46, a considerably small induction distance occur due to the post-shock temperature remaining significantly high up to some distance near the stagnation zone. Away from the stagnation line, the induction distance is increased as a result of decreasing shock strength and post-shock temperature.

Figure 6 shows comparison of enlarged contours of densities for Mach 5.11 and 6.46 which are magnifications of the circles in Figure 4(b) and Figure 5(b). There are wavy contours in the contours of density for Mach 5.11 whereas uniform contours for Mach 6.46. This denotes that

the instabilities in the reaction fraction disappear as the Mach number is increased from a C-J Mach number of 5.11 to a superdetonative Mach number of 6.46, keeping the same diameter. Thus, for the Mach number 6.46 case with the projectile diameter of 15 mm, both the bow shock and the reaction front have a smooth profile.

5. Conclusions

Adaptive Mixed Explicit-Implicit finite element method is applied to calculate the shock-induced combustion. The number of grid points needed to properly resolve the reaction front is greatly reduced due to the adaptive meshes.

The key parameters for the onset of periodic unsteadiness have been identified as induction time, reaction rate constant, activation energy, heat release, and projectile nose radius. In this study, the three cases have been simulated for Machs 4.18, 5.11, and 6.46 with a projectile diameter of 15 mm. Machs 4.18 and 5.11 show an unsteady reaction front, whereas Mach 6.46 represents a steady reaction front. Thus Chapman-Jouguet speed is one of deciding factor for the instabilities to trigger.

Reference

1. Cambier, J.L. and Anelman H., "Numerical Simulations of an Oblique Detonation Wave Engine," AIAA Paper 88-0063, January 1988.
2. White. M. E., Drummond J. p., and Kumar, Ajay. "Evolution and Status of CFD Techniques for Scramjet Applications." AIAA Paper 86-0160, January 1986.
3. Zeldovich. Y. B., and Shlyapintokh, I. Y., "Ignition of Explosive Gaseous Mixtures in Shock Waves." Office of Technical Services, U. S. Department of Commerce, Washington, DC, OTS: 50-41, 553, 1960
4. Lehr, H. F., "Experiments on Shock-Induced Combustion." Acta Astronautica, Vol. 17, September 1972, pp. 589-586.
5. Yungster, S., Eberhardt. S., and Bruckner, A. P., "Numerical Simulation of Shock-Induced Combustion by High-Speed Projectiles in Detonable Gas Mixture." AIAA Paper 89-0673, July 1989.
6. Lee, S. and Deiwert, G. S., "Calculation of Non-Equilibrium Hydrogen-Air Reaction with Implicit Flux Vector Splitting Method." AIAA Paper 89-1700, 1989.
7. Wilson, G. J. and MacCormack R.W., "Modelling Supersonic Combustion Using a Fully-Implicit Numerical Method." AIAA Paper 90-2307, July 1990.
8. Sussman, A. M. and Wilson, G. J., "Computation of Chemically Reacting Flow using a Logarithmic form of the Species Conservation Equations." Proceedings of Fourth International Conference on Numerical Combustion, Tampa, FL, December 2-4, 1991, pp. 224-227.
9. Matsuo, A. and Fujiwara T., "Numerical Simulations of Shock-Induced Combustion around an Axisymmetric Blunt Body." AIAA Paper 91-1414, June 1991.
10. McVey, J. B. and Toong, T. Y., "Mechanism of Instabilities of Exothermic Hypersonic Blunt-Body Flow." Combustion Science and Technology, Vol. 3, 1971. pp. 63-76.
11. Moon, S. Y. and Chung, T. J., Airbreathing Combustion in Shock Wave Turbulent Boundary Layer Interactions of High Speed Flows, *AIAA paper*, 94-2947, 1994.